Advances in Science and Technology Research Journal

Advances in Science and Technology Research Journal, 2026, 20(9), 13–24
https://doi.org/10.12913/22998624/221684
ISSN 2299-8624, License CC-BY 4.0

Received: 2026.04.16
Accepted: 2026.07.10
Published: 2026.08.01

Pareto-based design of electromagnetic air-core actuators: Integrating Biot–Savart law and finite element method verification

Zbigniew Pilch[1*], Maciej Gibas[1]

[1] Faculty of Electrical Engineering, Cracow University of Technology, Warszawska 24, Cracow, Poland
* Corresponding author's e-mail: zbigniew.pilch@pk.edu.pl

ABSTRACT

This article presents a methodology for optimizing the geometric parameters of air-core coils using the particle swarm optimization (PSO) algorithm. The design problem is formulated as a bi-objective task, aiming to maximize the magnetic flux density along the coil axis while simultaneously minimizing the conductor mass. An analytical model based on the Biot-Savart law was developed to drive the optimization process, allowing for the generation of Pareto fronts that illustrate the trade-off between magnetic performance and material consumption. To validate the proposed approach, five distinct design cases with varying geometric constraints were analyzed. The results obtained from the analytical model were verified against numerical simulations performed using the finite element method (FEM) in Agros2D software. The comparative analysis demonstrated high convergence between the analytical and numerical methods, with relative deviations remaining below 2.12%. The study confirms that the proposed hybrid methodology constitutes a robust tool for designing electromagnetic actuators, enabling the selection of optimal coil geometries that balance high magnetic force capabilities with lightweight construction.

Keywords: air-core coils, particle swarm optimization PSO, Biot-Savart law, finite element method, Agros2D, electromagnetic design, Pareto optimization.

INTRODUCTION

Air-core coils are an essential component of many electromagnetic systems, used in actuators, sensors, and wireless power transfer systems, among others [1]. However, their design involves the necessity of reconciling conflicting requirements – high magnetic flux density along the coil axis and minimal structural mass [2]. Classical analytical models, based on the Biot-Savart law, allow for rapid estimates and calculation of flux density values along the coil axis, but finding optimal solutions requires the application of other computational tools [3].

In the literature, the role of intelligent optimization methods in the design of electromagnetic systems is increasingly emphasized. Examples include works on linear induction machines, where the application of evolutionary algorithms enabled reduction of losses and mass while simultaneously increasing efficiency [4]. The application of similar approaches, such as particle swarm optimization (PSO), in optimizing the geometry of air-core coils allows for obtaining Pareto-optimal solutions, and their correctness can subsequently be verified using FEM simulations and experimental studies [5].

Air-core coils and their applications

Air-core coils, unlike coils with a ferromagnetic core, are characterized by simple construction and a linear relationship between current intensity and the generated magnetic flux density. The absence of a core eliminates hysteresis and magnetic saturation phenomena, which makes them particularly useful in systems requiring stable operating parameters [6].

Applications of air-core coils encompass a wide range of technical areas. In electronics, they are used as components of filters, resonant circuits, and antennas. In electrical engineering, they find application in systems exciting magnetic fields, including Helmholtz coils, used to generate uniform fields in laboratory research [7]. Such systems are utilized in magnetic sensor calibration, material property studies, and experiments on new functional structures, including magnetorheological materials [8].

In recent years, the growing importance of air-core coils in research on smart materials has been observed. Thanks to the possibility of precise magnetic field shaping, these coils allow for dynamic control of mechanical properties of materials. In medicine and NDT techniques, they are used for non-invasive structural examinations and in applications requiring controlled magnetic fields in confined spaces [9].

Optimization methods in coil design – the role of PSO

The design of electromagnetic coils requires consideration of multiple criteria simultaneously – from magnetic flux density values and its distribution within the coil, through energy efficiency understood as the amount of magnetic energy generated by the coil in its interior relative to the electrical energy supplied to the coil windings, to mass (significant in devices implementing motion) and manufacturing costs [10].

The magnetic field energy generated by an air-core coil is determined by Equation 1:

$$E_{mag} = \frac{1}{2} L I^2 \tag{1}$$

where: I – coil supply current [A], L – coil inductance [H], and the inductance of a coreless coil (solenoid) is calculated from Equation 2:

$$L = \mu_0 \frac{AN^2}{L_c} \tag{2}$$

where: μ_0 denotes the magnetic permeability of vacuum, A – coil cross-sectional area [m^2], N – number of coil turns [-], L_c – coil length [m].

After substituting (2) into (1) we have:

$$E_{mag} = \frac{1}{2} \mu_0 \frac{AN^2}{L_c} I^2 \tag{3}$$

Classical design approaches, based on the analysis of analytical relationships and gradient methods, often do not allow for finding globally optimal solutions, especially in the case of complex geometric and material constraints [11].

Algorithms inspired by natural phenomena, such as genetic algorithms, simulated annealing, or PSO, are widely described in the literature [12]. PSO in particular has gained popularity due to its implementation simplicity, small number of control parameters, and high effectiveness in multi-criteria problems. In coil design, it allows for simultaneously maximizing flux density along the coil axis and minimizing its mass, with the obtained solutions presented in the form of a Pareto front [13].

The role of PSO in electromagnetic engineering is becoming increasingly visible – this method finds application in the design of air-core coils, as well as electric machines and wireless power transfer systems. Optimization algorithms can be based on decision variable values calculated from analytical relationships (e.g., Biot-Savart law) or on values calculated using approximate methods - e.g., the finite element method. An important step is conducting experimental studies, which allow for confirming the results obtained by computational methods [14]. For example in [15], Chiarello and Malagoli presented a procedure for using the PSO algorithm in coil optimization for an electromagnetic actuator with four decision variables (electric current, number of turns, air gap and wire diameter).

MATERIALS AND METHODS

In order to perform optimization of air-core coil geometry, an integrated research procedure was developed encompassing analytical modeling, PSO algorithm, numerical simulations using the FEM. The research process was designed to enable comparison of results obtained at two levels:

- analytical model (exact solution), allowing for rapid estimation of flux density along the coil axis and its mass,
- numerical model, taking into account complete magnetic field analysis, implemented in the Agros2D software [16].

This chapter presents the successive stages of the adopted methodology: definition of the optimization problem and the adopted design space, construction of objective functions and constraints, implementation of the PSO algorithm along with Pareto analysis, as well as the scope of five analyzed geometric cases. Subsequently, the FEM simulation configuration is described.

Problem definition and design space

The aim of the research is to optimize the geometry of air-core coils in such a way as to obtain maximum magnetic flux density along the coil axis while simultaneously minimizing its mass. This is a classic multi-criteria problem in which conflicting requirements occur – increasing the number of turns or geometric dimensions usually leads to an increase in flux density, but simultaneously causes a significant increase in total mass. Increasing the winding wire diameter allows for supplying the coil with higher current, which increases the magnetic flux density value, but simultaneously, for a given coil volume, decreases the number of turns. One must also remember the aspects of thermal phenomena resulting from the flow of current through the coil windings [17].

The design space was determined by three main geometric dimensions:

- coil inner diameter – D_{in},
- coil outer diameter – D_{out},
- winding height – L_c.

In all calculations, it was assumed that all considered coil cases (Case 1–5, described in detail in Section 2.4) are wound with wire of 0.8 mm diameter and supplied with a current of 2 A intensity.

Figure 1 presents a cross-section of a cylindrical coil used as an electromagnetic field excitation in an MR fluid clutch. The figure should be treated as an axial cross-section showing the section up to the axis of symmetry (the axis of symmetry is the z-axis). Geometric dimensions are marked in the figure.

Based on these parameters, the number of turns resulting from the selection of copper winding wire diameter and the total conductor mass are determined. The ranges of dimensional variability were selected to cover five optimization variants (Case 1–5, described in detail in Section 2.4), encompassing different design space configurations – from compact coils with small dimensions to larger constructions intended for generating stronger magnetic fields. An additional constraint is the minimum spacing between the inner and outer diameter, equal to at least twice the wire diameter, which ensures the physical correctness of the solution.

Objective function and analytical model

The optimization task was formulated as a two-criteria problem in which two conflicting objectives are considered:

1. Maximization of the axial component value of magnetic flux density along the coil axis. The flux density along the air-core coil axis (at the coil's central point) was calculated based on the Biot-Savart law. For a single turn with radius R, through which current I lows, the flux density value at distance z from the turn plane is described by Equation 4:

$$B_z = \frac{\mu_0 I R^2}{2(R^2 + z^2)^{3/2}} \tag{4}$$

where: μ_0 denotes the magnetic permeability of vacuum, I – coil supply current [A], R – winding radius of a single coil turn [m], z – distance from the geometric center of the coil, measured along the coil axis [m].

For a coil composed of N turns, with height L_c, inner diameter D_{in} and outer diameter D_{out}, the total flux density along the axis is the sum of contributions from individual turns, uniformly distributed along the axis and radius:

$$B_{zC} = \sum_{i=1}^{N} \frac{\mu_0 I R_i^2}{2(R_i^2 + z_i^2)^{\frac{3}{2}}} \tag{5}$$

where: R_i and z_i denote the radius and axial position of the i-th turn, respectively.

2. Minimization of coil mass.

The conductor mass was calculated as:

$$m = \rho \cdot l \cdot A \tag{6}$$

where: ρ – copper density (8.96 g/cm^3), $l = N \cdot 2\pi R_{avg}$ – total wire length, where $R_{avg} = \frac{D_{in} + D_{out}}{4}$, $A = \frac{\pi d^2}{4}$ – wire cross-sectional area with diameter d.

The optimization problem for the air-core coil was formulated considering two criteria:

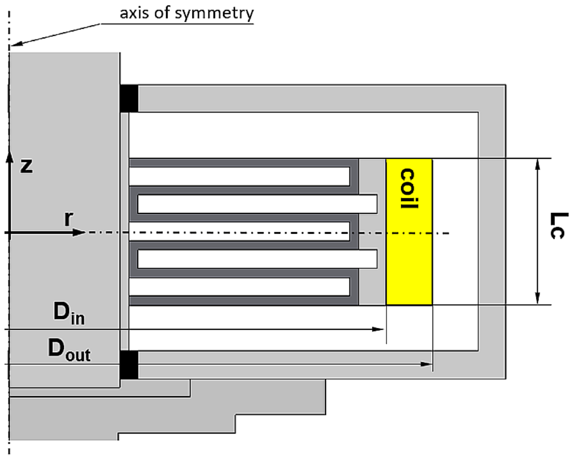

Figure 1. Axisymmetric Cross-sectional view of the MR clutch – an example of using an electromagnetic coil

$$maxB_{coil}(D_{in}, D_{out}, L_c)$$
$$minm(D_{in}, D_{out}, L_c) \tag{7}$$

The first criterion is understood as achieving the maximum peak value of the axial component of magnetic flux density. The second criterion is understood as the minimum coil mass value – the winding wire mass.

It should be noted that the analytical model based on the Biot-Savart law involves several simplifying assumptions that define the scope of its applicability: (1) the finite thickness of the conductor cross-section is neglected, with each turn modeled as an ideal current loop; (2) the effects of current density distribution and Joule heating within the windings are not taken into account; (3) the analysis is limited to the axial component of magnetic flux density along the coil axis, and off-axis field errors are not evaluated. These assumptions are well-justified for the purpose of iterative geometry optimization, where computational speed is critical, and are consistent with the standard application of the Biot-Savart law in the literature. The FEM model in Agros2D, used for final verification, does not rely on these simplifications and accounts for the full spatial distribution of the magnetic field.

PSO algorithm configuration (parameters, fitness function, Pareto analysis)

To solve the defined problem, the PSO algorithm was applied, inspired by the flocking behaviors of birds and fish. Each solution (swarm particle) represents a vector of geometric coil parameters:

$$x_i = (D_{in}, D_{out}, L_C) \tag{8}$$

where: i = 1,2, ..., N_p denotes the particle number in a population of size N_p.

The movement of particles in the solution space is defined by velocity and position update equations:

$$v_i(t+1) = wv_i(t) + c_1r_1\big(p_i - x_i(t)\big) + \\ +c_2r_2(g - x_i(t)) \tag{9}$$

$$x_i(t+1) = x_i(t) + v_i(t+1) \tag{10}$$

where: *w* – inertia coefficient, controlling the influence of velocity from the previous iteration, c_1, c_2 – acceleration coefficients (cognitive and social factors, respectively), r_1, r_2 ~ U(1.0) – random numbers generated in each iteration, p_i – best solution found so far by the i-th particle, g – global best solution in the population. t – computational step,t + 1 – next computational step.

To avoid premature convergence, adaptive control of parameters w, c_1, c_2 was applied, and in some iterations, random mutation of particle positions was introduced, which increased solution diversity and improved exploration of the design space (solution set).

Since the task is multi-criteria, each vector x_i was evaluated based on two indicators:
- axial component of magnetic flux density along the coil axis B_{ZC} (maximum value of this component),
- minimum coil mass value – winding wire mass m.

Solutions were compared in the sense of Pareto dominance: solution x_a dominates x_b if:

$$f_k(x_a) \leq f_k(x_b), \forall k \in \{1,2\},$$
$$and\ \exists k: f_k(x_a) < f_k(x_b) \tag{11}$$

In this way, a Pareto front was constructed, illustrating the compromise between flux density increase and mass reduction.

In the studies, the following were adopted:
- population size: N_p = 50,
- maximum number of iterations: T = 200,
- inertia coefficient: w ∊ [0.4, 0.9] (decreasing linearly),
- acceleration coefficients: c_1 = c_2 = 2.0,
- mutation probability: p_m = 0.1.

Such a configured algorithm ensured balance between exploration (global search) and exploitation (refinement of solutions in the neighborhood of the optimum).

Five optimization cases

To analyze the impact of geometric constraints on the compromise between the axial component value of magnetic flux density and coil mass, five experiments (Case 1–5) were conducted, differing in the ranges of design parameters: inner diameter D_{in}, outer diameter D_{out}, and winding height L_c. In all cases, geometric and technological correctness conditions were enforced. Table 1 summarizes the ranges of upper and lower limits for decision variable values.

Thanks to this division, it was possible to examine how the range of permissible dimensions affects the distribution of Pareto solutions and the compromises between the axial component of magnetic flux density along the coil axis B_{Zc} and coil mass minimization m.

The described optimization task was implemented in the form of an application. The application was prepared in the MATLAB environment using the App Designer module. The user interface (Figure 2) consists of three main functional areas:

- Control panel – enables selection of the analyzed optimization case (Case 1–5) and launching of the PSO algorithm. Buttons are also available to run all cases simultaneously, stop calculations, export results, and generate the Pareto front.
- Results panel – displays values obtained in successive iterations, including the best solutions so far and geometric parameters corresponding to points from the Pareto front.
- Visualization panel – presents the distribution of Pareto fronts and the course of the optimization process in the form of graphs, which facilitates interpretation of compromises between flux density maximization and mass minimization.

Thanks to this structure, the application enables full control over the course of calculations and intuitive comparison of results obtained for different design space configurations. From the convergence course, it can be seen that despite the adopted maximum number of iterations: T = 200, the result stabilizes its value after approximately 30–40 iterations. Figure 3 presents the calculation results performed for the 3rd case (case 3). On the left side, the Pareto front points between Bz and m are presented.

Analysis of Pareto fronts for all five cases allowed for unambiguous indication of optimal weights in the objective function. Adopting values of $w_B = 0.7$ for flux density and $w_M = 0.3$ for mass ensured the best compromise between the conflicting requirements described by Equation 7. In each of the analyzed cases, the point corresponding to these weights was located in the area of the Pareto front where a significant increase in flux density was obtained with only a moderate increase in mass. For cases 1 and 2, these weights allowed for a clear increase in magnetic field value compared to very light initial constructions. In cases 3 and 4, the 0.7/0.3 optimum gave high flux density close to the maximum value, with mass maintained at an acceptable level, which was also confirmed by analysis of the Score(w1) indicator, defined as $\mathrm{Score}(w1) = w1 \cdot \hat{B}zC - (1-w1) \cdot \hat{m}$, where $\hat{B}zC$ and $\hat{m}$ denote normalized values of flux density and mass respectively, and w1 is the weight assigned to the flux density criterion. In case 5, the flux density preference at 0.7 level ensured a favorable compromise, avoiding

Table 1. Dimensional ranges adopted in the five analyzed optimization cases

Case	[mm]	D_{out} [mm]	L_c [mm]	Case characteristics
Case 1	25–45	45–65	25–45	A
Case 2	5–25	15–35	5–25	B
Case 3	45–65	75–95	35–55	C
Case 4	25–35	65–95	20–40	D
Case 5	25–45	35–55	35–55	E

Note: Case characteristics: A – Medium dimensions; balanced B/mass compromise,
B – Very compact coils for precision applications, emphasis on low mass,
C – Larger windings generating high B, D – Slender, wide winding; high D_{out} with moderate D_{in},
E – High windings in medium diameters; h limit test.

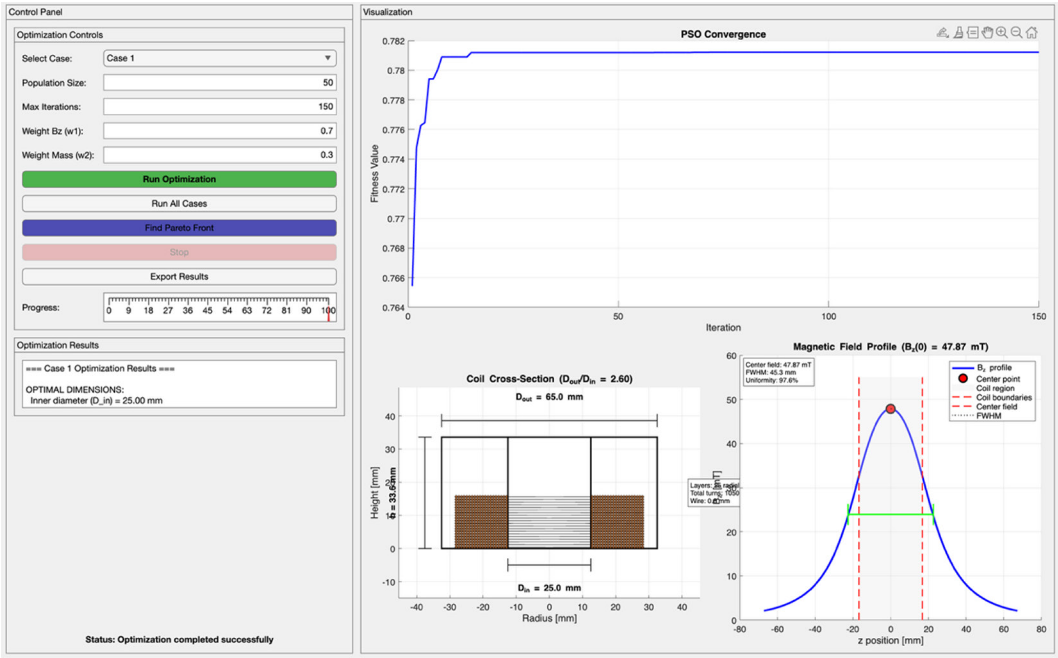

Figure 2. GUI interface of an application that optimizes the shape of an air coil using the PSO algorithm

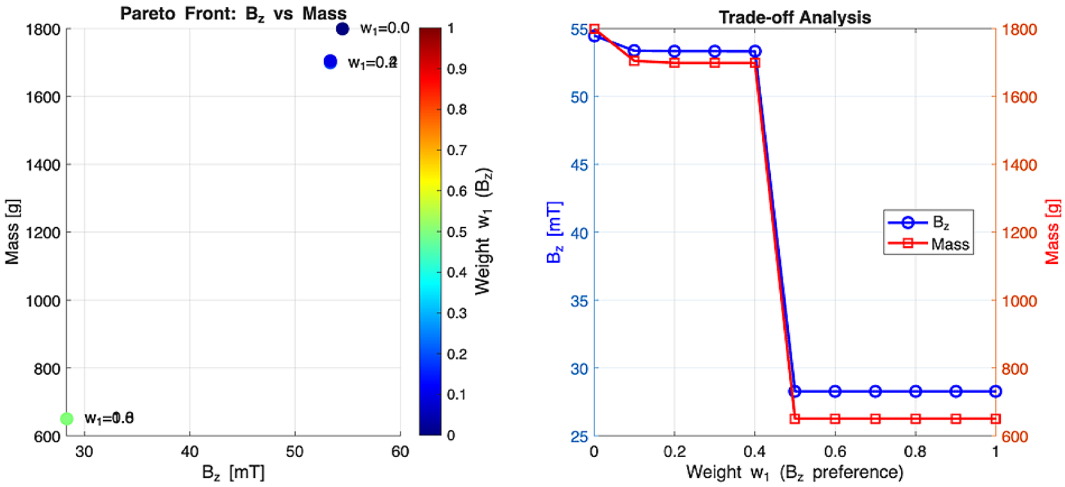

Figure 3. Example Pareto analysis for "Case 3"

both too low field value (for smaller weights) and unprofitable mass increase (for larger flux density weights). This choice can therefore be considered most appropriate for further analyses and numerical comparisons. Calculation results for all 5 cases are presented in Figure 4.

Figure 4 presents a summary of results obtained within the five optimization cases conducted, illustrating both the distribution of Pareto solutions and key geometric dependencies, as well as the course of PSO algorithm operation. On the three-dimensional graph Figure 4a, the solution space is visible, in which electromagnetic flux density values along the coil axis are marked in color. Analysis of this area clearly indicates that the highest flux density values are obtained for configurations with larger outer diameter and winding height, while maintaining moderate inner diameter. The relationship between flux density value and mass presented in the bar chart Figure 4b confirms that in the third and fourth cases, the highest magnetic field values were obtained, however, in the third case, this came at the cost of significantly higher mass. Analysis of the efficiency indicator defined as the ratio of flux density to conductor mass Figure 4c indicates that the

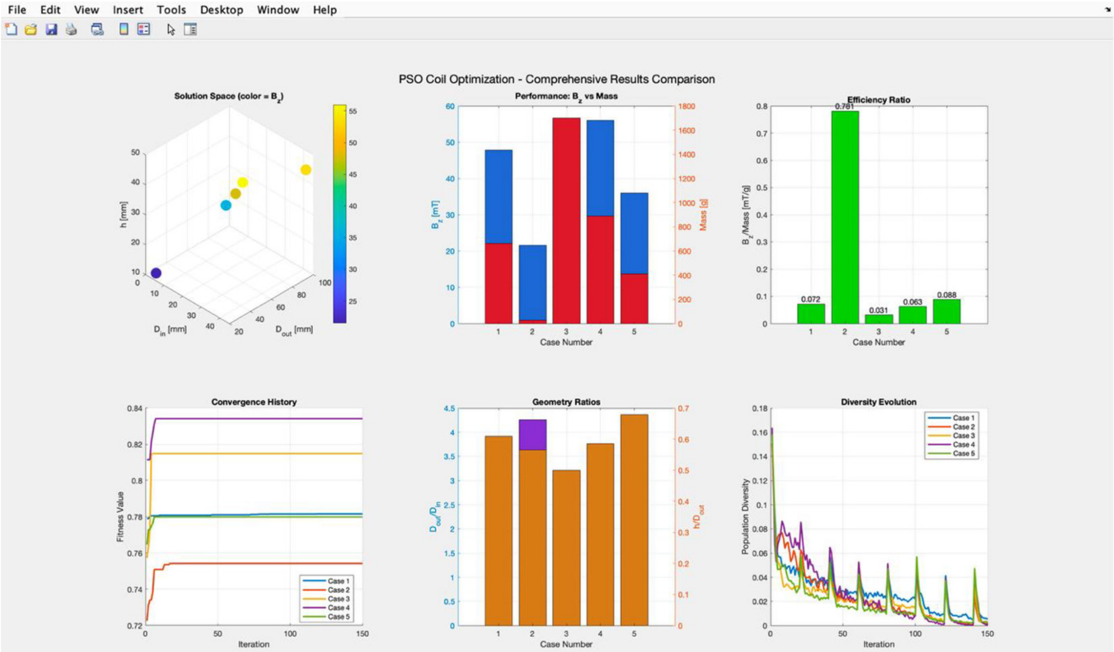

Figure 4. Summary of calculation results performed with the developed calculation program for the five studied cases

best material effectiveness is provided by the second case, in which compact geometry allows for achieving a favorable compromise between low mass and useful field level. The convergence history Figure 4d confirms stable algorithm operation in all cases – fitness function values stabilize after several dozen iterations, and the calculation course shows no signs of oscillations or instability. Additional information is provided by geometric proportion graphs Figure 4e, which show that optimal configurations are characterized by an outer to inner diameter ratio of approximately 3–4.5 and a height to outer diameter ratio in the range of 0.55–0.70. The last graph Figure 4f illustrates the evolution of population diversity – periodic increases resulting from mutation introduction are visible, which allows avoiding premature convergence and increases the chance of exploring globally favorable solutions. The entire analysis leads to the conclusion that the fourth case represents the most balanced compromise between high flux density and moderate mass, while the second case stands out with the highest efficiency in terms of material utilization.

FEM numerical analysis of flux density distribution in the air-core coil using Agros2D software

The results obtained from calculations with the program developed in the MATLAB environment using the App Designer module were decided to be compared with results obtained from field calculations. The purpose of these simulations is to obtain information about the distribution of magnetic flux density in the area inside the coil (not only along the coil axis) and around it. Agros2D software [16] was used for calculations, which enables analysis of electromagnetic phenomena in axisymmetric systems, which allowed for significant reduction in the number of mesh elements while maintaining high accuracy in field distribution representation. The mesh was generated automatically with adaptive refinement in areas with the highest magnetic flux density gradients, particularly in the conductor region and along the coil axis.

Figure 5 presents a color map of magnetic flux density value distribution and field isolines in the area around the coil for optimal coil dimensions according to Case 3 (Table 2) (D_{in} = 45 mm, D_{out} = 93.19, L_c = 26.44). In the simulation, it was assumed that the coil windings were made with winding wire of 0.8mm diameter and are supplied with a current of 2A intensity.

For finite element mesh generation, the mesh refinement parameter was set to 2 in Agros2D. Approximately 16,770 finite elements are generated for the entire domain. Figure 5 shows the appearance of the finite element mesh - at the top the initial mesh, and at the bottom the solution mesh. As part of the analysis, the distribution of the magnetic flux density vector in the coil surroundings and the detailed course of the axial component Bz along the axis of symmetry were determined. The results were later compared with analytical calculations for the coil's central point. Additionally, numerical field profiles enabled more accurate assessment of flux density distribution uniformity and the influence of geometric dimensions on local values outside the coil center, which is not possible to capture in the analytical model. The use of FEM simulation also allowed for verification of the influence of adopted geometric constraints on Pareto front formation. It was demonstrated that variants indicated by the PSO algorithm as optimal were characterized by a favorable compromise between field value along the axis and total conductor mass also from the numerical perspective, which constitutes significant confirmation of the proposed methodology's effectiveness.

RESULTS

The developed computational tool allowed for carrying out the process of selecting coil dimensions meeting two established optimization criteria. Based on adopted assumptions – e.g., the range of coil dimension variability (D_{in} , D_{out}, L_c), the dimension optimization process was carried out using the PSO method while satisfying criteria (7) and (11), and then for such calculated coil dimensions, calculations of flux density distribution in the coil area and beyond were performed using two methods. The results were compared. The presented computational tools (Biot-Savart model, PSO algorithm, FEM) can be combined into one procedure sequence, which is presented in Figure 6.

This chapter presents the results of conducted research encompassing optimization of air-core coil geometry using the PSO method, comparison of obtained results using the finite element method in Agros2D software. Results analysis began with five optimization cases (Case 1–5), in which different ranges of geometric dimensions were considered, sufficiently different to lead to different optimal solutions, which allowed for assessment of the influence of the adopted design space on the distribution of Pareto fronts and the compromise between magnetic flux density value and conductor mass. Subsequently, results obtained in the analytical model were compared with numerical simulation results. Such an approach enabled comprehensive assessment of the proposed methodology's effectiveness and confirmation of its correctness.

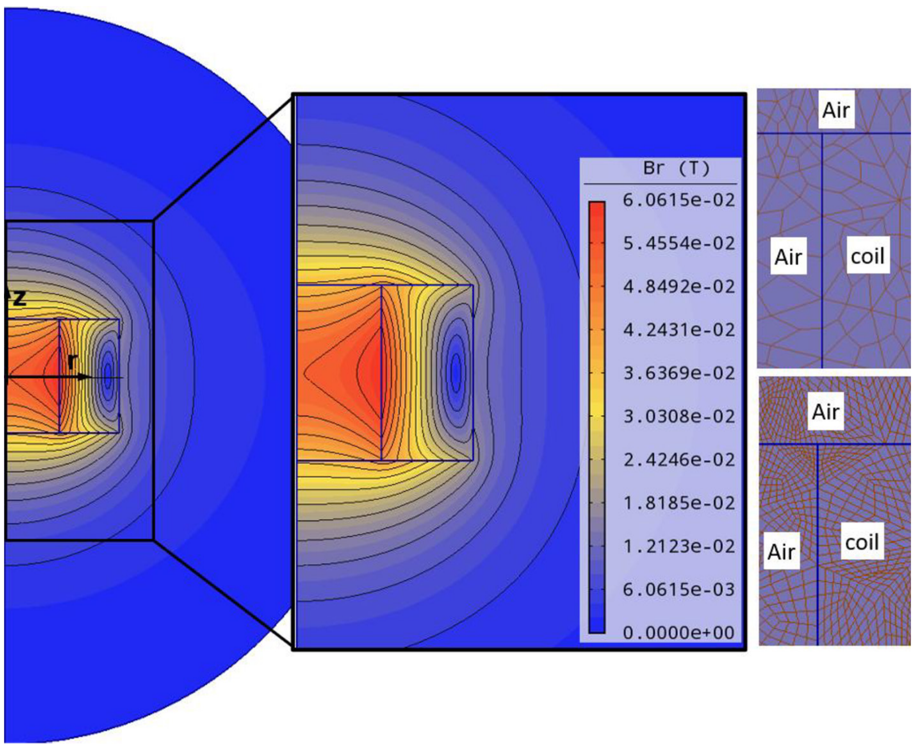

Figure 5. Results of the analysis of the distribution of magnetic induction values and field isolines in the area around the coil for optimal coil dimensions according to Case 3

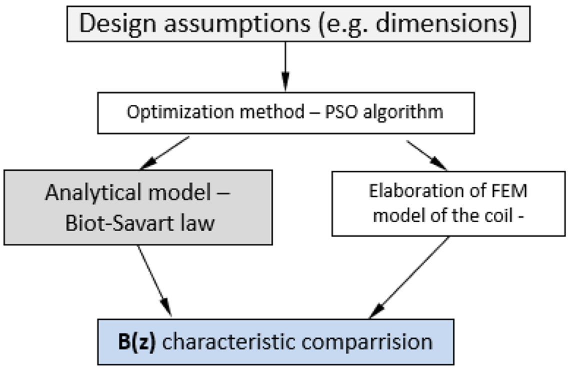

Figure 6. Computational methods useful in developing structures with air coils

PSO optimization results (Case 1–5)

Within the five analyzed cases, Pareto-optimal solutions were obtained corresponding to different geometric coil configurations. For each case, the PSO algorithm returned a set of parameters describing the inner and outer diameter, winding height, number of turns, and total conductor mass, as well as magnetic flux density values along the axis and fitness indicators. The results are summarized in Table 2, which presents both geometric quantities and solution quality assessment indicators.

Analysis of the obtained results shows clear differences between individual cases. The first variant represents medium winding dimensions and provides flux density of 47.9 mT with a mass of 675 g. The second case, characterized by very small geometric dimensions, achieved the lowest flux density value (21.3 mT), but at the same time is distinguished by the highest material efficiency, expressed by the B_{zCmax}/m indicator. The third case allowed for obtaining high flux density (53.32 mT), however, with very large conductor mass exceeding 1.6 kg, which limits its practical usefulness. The most favorable compromise is revealed by the fourth case, in which the highest fitness function value (0.83) was obtained, combining high flux density (55.9 mT) with mass maintained at an acceptable level (890 g). The fifth case represents a construction with increased height, giving flux density of 35.9 mT with mass of approximately 409 g, which places it as an intermediate solution between compact and heavy windings. Comparison of all cases confirms that weight preference $w_B = 0.7$ and $w_M = 0.3$ leads to obtaining solutions characterized by high field value with controlled conductor mass.

Analytical calculation results for optimal dimension values D_{in}, D_{out}, L_c (Case 1–5)

Figure 7 presents characteristics of magnetic flux density distribution for the 5 considered cases. Calculations were performed using the analytical method based on Equation 4. Dashed lines indicate the coil outline. The quantity "Field" denotes the definite integral of the axial magnetic flux density along the coil axis over the coil length, defined as Field = $\int Bz(z)\,dz$, where the integration is performed over the coil length Lc. For improved readability, the units in the graphs were changed from T to mT and from m to mm.

Comparison of the analytical model and FEM

The field model developed in the Agros2D software was used to compare the results obtained with this computational method against the analytical model, which in this case is treated as the exact solution (reference point). Furthermore, the model developed and verified at this stage can be used in the process of designing and constructing technical devices in which solenoids are utilized. Figure 8 presents an example comparison of the magnetic flux density distribution in the coil calculated from the Biot-Savart model and the results obtained from the Agros2D simulation for CASE3. A clear agreement between the curves is visible—both the values from the analytical model and those calculated using the FEM indicate a monotonic decrease in magnetic flux density with increasing distance from the coil surface. The convergence of the results is at a very good level; in the worst case, the deviation does not exceed 2.12% maximum point value of induction $B_{zC\text{-}max}$ on the coil symmetry axis (Case 2). The flux density distribution is shown not only within the coil area itself (its span is depicted in Figure 8 by vertical dashed lines and additionally labeled as "coil edges") but also outside the coil outline.

Table 3 summarizes the results obtained from the analytical calculations (the Biot-Savart formula), the values calculated by the PSO algorithm for the optimal solutions according to the criterion described by Equation 11, and the results derived from the field models built using the dimensions obtained from the PSO algorithm. The maximum magnetic flux density values acquired through the compared methods were juxtaposed.

Table 2. Summary of parameters for P1-P5 – optimal values and coil mass, maximum flux density along the coil axis calculated using the PSO method

Optimal value according to PSO					
Case	D_{in}	D_{out}	L_c	Mass m	Induction B_{zCmax}
	[mm]	[mm]	[mm]	[g]	[mT]
1	25	64.41	36.17	675.42	47.91
2	5	21.91	12.02	27.59	21.34
3	45	93.10	46.45	1698.74	53.32
4	25	68.45	40.00	890.12	55.94
5	25	53.52	35.36	408.52	35.86

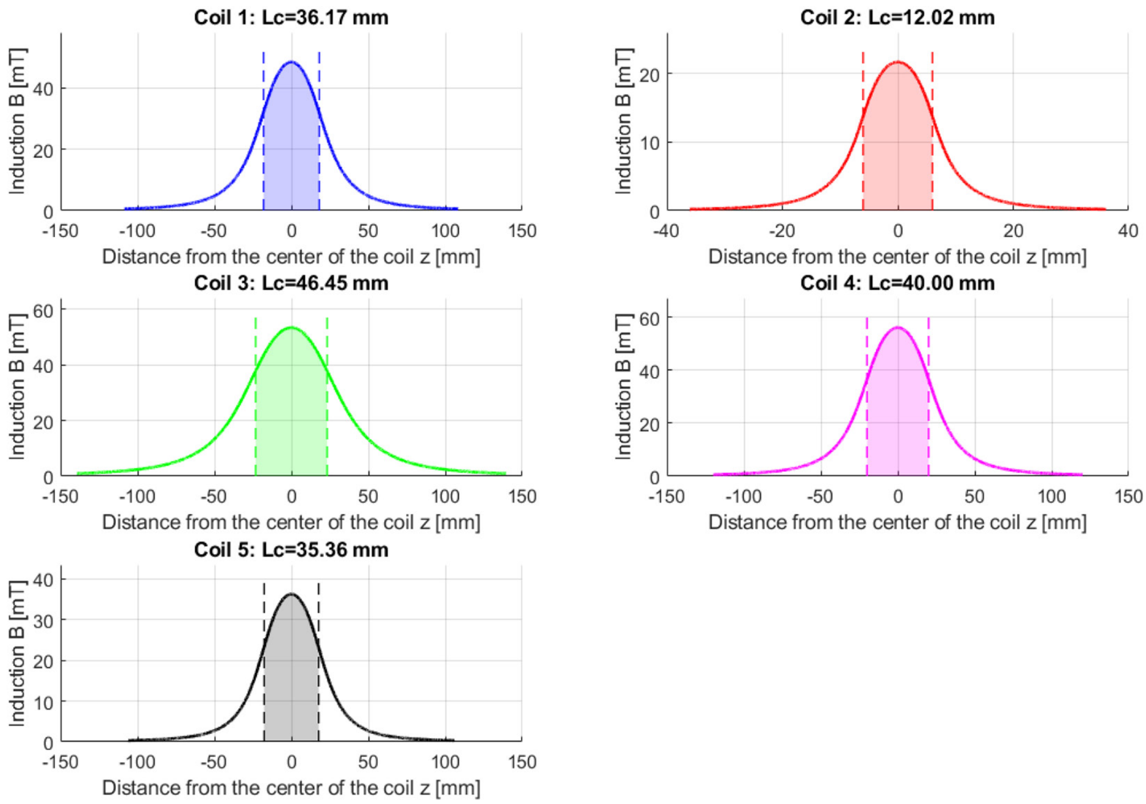

Figure 7. Characteristics of the magnetic induction values along the axis of air coils according to Case 1–5

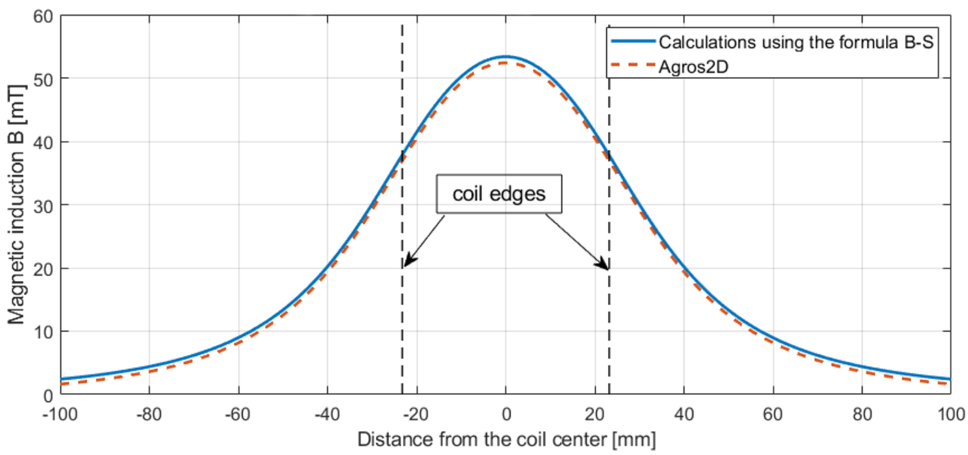

Figure 8. Comparison of analytical (Biot-Savart) and FEM simulation results for Case 3

Table 3. Comparison of B_{zCmax} results obtained using the analytical method and FEM calculations and the magnetic energy generated inside the coil volume

Case	Analit. method	MES	Difference col. 3 to 2	Magnetic energy
	mT	mT		J
Case 1	48.3	47.67	-1.32%	$1.41*10^{-2}$
Case 2	21.69	21.24	-2.12%	$3.52*10^{-5}$
Case 3	53.30	52.38	-1.73%	$7.75*10^{-2}$
Case 4	56.02	55.63	-0.70%	$2.08*10^{-2}$
Case 5	36.23	35.72	-1.41%	$7.73*10^{-3}$

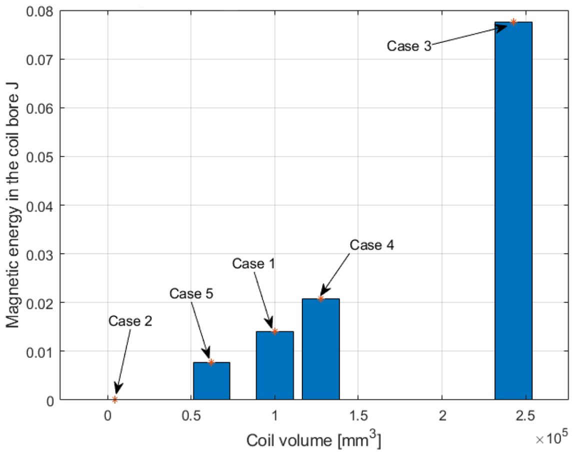

Figure 9. Magnetic energy in the coil bore vs to the coil volume

Data analysis indicates a good agreement between the analytical calculations and the FEM results. For Case 1, the difference between the analytical method (48.30 mT) and the FEM simulation (47.67 mT) is slightly over 1.3%. A similar situation is observed in Case 2, where the deviation slightly exceeds 2%. Similarly, for Case 3, the discrepancy between the maximum flux density calculated analytically and that calculated using the finite element method is approximately 1.73%. For Case 4, the difference between the FEM results and the PSO remains small – only 0.7%. Finally, for Case 5, the difference in the results is slightly over 1.4%. In summary, the presented comparison demonstrates high consistency among the analytical results, the PSO algorithm calculations, and the FEM. The largest differences occur in cases with a wider range of geometric dimensions, but they do not exceed the typical level for simplified models. Ultimately, the obtained results confirm the reliability of the adopted methodology and the correct implementation of the optimization algorithm. Data analysis revealed a very good agreement in the curve shapes across all three models. Differences in absolute values were within the range of slightly over 2%, which can be attributed to numerical errors. Simultaneously, it was confirmed that the point corresponding to the weights w_B = 0.7 and w_M = 0.3 lies in the region providing the most favorable compromise between the flux density and the conductor mass, also in the real system. Figure 9 presents a comparison of the magnetic energy generated by the sample coils relative to the volume of the winding wire.

CONCLUSIONS

The conducted research confirmed the effectiveness of applying the PSO algorithm in the multi-objective optimization process of air-core coils. The proposed methodology enabled effectively finding a compromise (Pareto front) between maximizing the axial component of the magnetic flux density (B_{zCmax}) and minimizing the winding mass (m). Based on the obtained results and physical analysis, the following conclusions were drawn:

Model verification: The comparison of the results obtained from the analytical model (Biot-Savart law) with the FEM field simulations (Agros2D) showed high agreement, with relative errors not exceeding 2.12% for all five analyzed cases (Case 1–5). This confirms that the fast analytical model is sufficient for iterative optimization calculations, while computationally expensive FEM simulations can be used solely for final verification.

Optimal geometry: It has been demonstrated that the most favorable compromise between the parameters (weights w_B 0.7; w_M = 0.3) is achieved for designs with an outer-to-inner diameter ratio in the range of 3.0–4.5. This allows for avoiding the oversizing of the structure while maintaining high field parameters. Flux density – Energy – Force relationship: The analysis of the magnetic energy stored in the internal volume of the coil (Figure 9) indicates a direct correlation with the determined magnetic flux density. According to the relationship $\mathrm{E_{mag}} \propto \mathrm{B}^2$, maximizing the flux density along the coil axis leads to a quadratic increase in the field energy density. This is crucial in the design of electromagnetic actuators, because the force acting on a ferromagnetic element (e.g., an armature or plunger) introduced inside the coil is directly proportional to the gradient of this energy ($\mathrm{F} = \nabla \mathrm{E_{mag}}$). Thus, optimizing the geometry to maximize B_z with a constrained mass is equivalent to optimizing the useful force of the actuator relative to its own weight.

Applicability: The presented approach constitutes a universal engineering tool that can be directly applied in the design of actuating systems, magnetorheological clutches, and magnetic separation systems, where a high force density while maintaining compact dimensions is crucial. It should be noted that the results presented here are limited to air-core configurations, and extension to systems with ferromagnetic cores would require incorporation of material nonlinearities (e.g., B-H curves and magnetic saturation), which falls outside the scope of the present study and represents a direction for future work.

REFERENCES

1. Budinger, V., Bouzidi, Y., Alves, F. Contactless power supply for moving sensors and actuators in high-precision mechatronic systems with long-stroke power transfer capability in x–y plane. Sensors and Actuators A: Physical 2008, 143(2), 379–387. https://doi.org/10.1016/j.sna.2007.12.012
2. Zhu, X., Xing, M., Ye, J., Liu, X., Ren, Z. Design and optimization of a novel solenoid with high magnetic uniformity. Scientific Reports 2024, 14, 24650. https://doi.org/10.1038/s41598-024-76501-y
3. Zolfaghari, H. Integrated analytical modeling and numerical simulation for electromagnetic soft actuators. Micromachines 2025, 14(3), 128. https://doi.org/10.3390/mi14030128
4. Wogi, L., Thelkar, A., Tahiro, T. S., Ayana, T., Urooj, S., Larguech, S. Particle swarm optimization based optimal design of six-phase induction motor for electric propulsion of submarines. Energies 2022, 15(9), 2994. https://doi.org/10.3390/en15092994
5. Wu, W., Zhou, B., Liu, Z., Jing, W., et al. Design of highly uniform magnetic field coils based on a particle swarm optimization algorithm. IEEE Access (do publikacji online: August 2019). https://doi.org/10.1109/ACCESS.2019.2933608
6. Lu Wan, Khilnani A. D., Wu X., Liu X., Pignari S. A., Thomas D. W. P., Sumner M., Grassi F. Optimal design of single-layer and multi-layer air-core inductors considering uncertainty factors. IEEE Access 2023, 11. https://doi.org/10.1109/ACCESS.2023.3336572
7. Zhai, L., Song, G., Wang, T., Xu, L. Design method of wide-band high-current air-core inductor. IET Power Electronics 2022, 15(6), 1205–1212. https://doi.org/10.1049/pel2.12341
8. Mahavarkar, P., John, J., Dhapre, V., Dongre, V., Labde, S. Tri-axial square Helmholtz coil system at the Alibag Magnetic Observatory: upgraded to a magnetic sensor calibration facility. Geoscientific Instrumentation, Methods and Data Systems 2018, 7, 143–149. https://doi.org/10.5194/gi-7-143-2018
9. Phu, D. X., Choi, S.-B. Magnetorheological fluid based devices reported in 2013–2018: Mini-review and comment on structural configurations. Frontiers in Materials 2019, 6, 19. https://doi.org/10.3389/fmats.2019.00019
10. Pateri, E., Sabug Jr., L., Ruiz, F., Gruosso, G. (2024). Efficient multi-objective optimization framework for induction heating systems design. IEEE Access 2024, 12, 95347. https://doi.org/10.1109/ACCESS.2024.3425933
11. Reznichenko, I., Erlich, I., Váncza, J. Magnetic coil's performance optimization with nonsmooth heuristic methods to overcome gradient-based limitations. Mathematics 2025, 13(15), 2490. https://doi.org/10.3390/math13152490
12. Wadhwa, R. S. Electromagnet Shape Optimization using Improved Discrete Particle Swarm Optimization (IDPSO). In: Proceedings of the COMSOL Conference 2012, Milan, Italy.
13. Rahmat-Samii, Y. Particle swarm optimization in electromagnetics. IEEE Transactions on Antennas and Propagation 2004, 52(2), 397–407. https://doi.org/10.1109/TAP.2004.823969
14. Gádor, K., Kocsis, J., Lévai, P., Benedek, Z. (2021). Robust and multi-objective pareto design of a solenoid. Electronics, 2021, 10(17), 2139. https://doi.org/10.3390/electronics10172139
15. Chiarello, E.; Malagoli, J. A. Optimal coil design of an electromagnetic actuator using particle swarm optimization. Journal Européen des Systèmes Automatisés 2020, 53(6), 755–761. https://doi.org/10.3166/jesa.53.755-761
16. Available online: http://www.agros2d.org/ (accessed on 10 April 2026).
17. Kluszczyński, K., Pilch, Z. A Comparison study on magnetorheological multi-disc clutches in steady continuous-duty states from the viewpoint of electrical energy consumption and spatial temperature distribution. Appl. Sci. 2022, 12, 7895. https://doi.org/10.3390/app12157895